Critical currents, flux-creep activation energy, and potential barriers for the vortex motion from flux-creep experiments

I. L. Landau[1,2] and H. R. Ott[1]
[1]*Laboratorium für Festkörperphysik, ETH Hönggerberg, CH-8093 Zürich, Switzerland*
[2]*Kapitza Institute for Physical Problems, 117334 Moscow, Russia*
(Received 16 October 2000; published 20 April 2001)

We present an experimental study of thermally activated flux creep in a superconducting ring-shaped epitaxial $YBa_2Cu_3O_{7-x}$ film as well as a different way of analyzing the experimental data. The measurements were made in a wide range of temperatures between 10 and 83 K. The upper temperature limit was dictated by our experimental technique and at low temperatures we were limited by a crossover to quantum tunneling of vortices. It is shown that the experimental data can very well be described by assuming a simple thermally activated hopping of vortices or vortex bundles over potential barriers, whereby the hopping flux objects remain the same for all currents and temperatures. This procedure of data analysis also allows us to establish the current and temperature dependencies of the flux-creep activation energy U, as well as the temperature dependence of the critical current I_c, from the flux-creep rates measured at different temperatures. The variation of the activation energy with current, $U(I/I_c)$, is then used to reconstruct the profile of the potential barriers in real space.

DOI: 10.1103/PhysRevB.63.184516 PACS number(s): 74.72.Bk, 74.60.Ge, 74.60.Jg, 74.76.Bz

I. INTRODUCTION

Investigations of the flux-creep process in type-II superconductors reveal important information about the interaction of vortices with pinning centers and among the vortices themselves. Studies of this type are especially rewarding for high-temperature superconductors (HTSC's) because in these materials a particularly rich variety of features of the vortex state has been established. In principle, the analysis of flux-creep data obtained at different temperatures permits to establish the dependence of the flux-creep activation energy U on the current density j and on temperature T. Different scaling procedures have been developed and used in order to deduce this information.[1–15,19] However, the interpretation of the experimental results is rather complicated because the suggested procedures involve many parameters which are not *a priori* known. Actually, there is no way to deduce all the parameters from the experimental data alone and some additional assumptions have to be made. The lacking input is usually provided by invoking different theoretical models and therefore the final result naturally depends on the particular chosen model. In many cases, different models have been employed to interpret data obtained from the same kind of samples, resulting, for example, in rather differing $U(j)$ curves. This is why, in spite of the extensive literature on this subject, the available information following from the analyses of the experimental data is still, to a certain degree, inconclusive and often controversial.

Recently we have proposed a different approach for analyzing the flux-creep rates in HTSC's.[20] This approach is based on a few basic assumptions and it essentially consists in merging the experimental voltage-current (V-I) characteristics of one sample, obtained at different temperatures, using their shape as the key to deduce the scaling parameters. It has been demonstrated that this approach works rather well for V-I characteristics of a ring-shaped film of $YBa_2Cu_3O_{7-x}$ (YBCO) in the temperature range between 10 and 60 K, the temperature interval covered in the work previously published in Ref. 20. The proposed scaling procedure permits us to establish the dependence of the flux-creep activation energy U on the normalized current density j/j_c, where j_c is the critical current density, as well as the temperature dependence of the critical current, directly from the V-I characteristics of the sample in the flux-creep regime. The main goal of the present work was to test whether the same procedure may also be applied successfully at temperatures closer to T_c. Therefore we have rearranged the experimental setup such as to allow an extension of the measurements up to 83 K. This extension of the measurements to higher temperatures is important because it provides information about $U(j/j_c)$ for low values of j/j_c. In this way the covered range of currents has been extended down to $j/j_c \approx 0.05$, approximately an order of magnitude lower than $j/j_c \approx 0.4$, reached in Ref. 20.

In addition to monitoring the current decay in zero external field as described in Ref. 20, we have extended the database by measuring the flux-creep rates also in external magnetic fields of 0.3 and 1 kOe.

II. EXPERIMENT

A. Sample and measurements

The experiments have been made using a ring-shaped epitaxial YBCO film with a superconducting critical temperature $T_c = 87.5$ K. The external diameter of the ring is 10 mm and its width is approximately 2 mm. The film thickness is about 0.3 μm. The resistive transition to superconductivity of the sample is shown in the inset of Fig. 3. More details about the sample and the basic experimental setup can be found elsewhere.[20–22]

For the present study we intended, as mentioned above, to extend the measurements to temperatures as close to T_c as

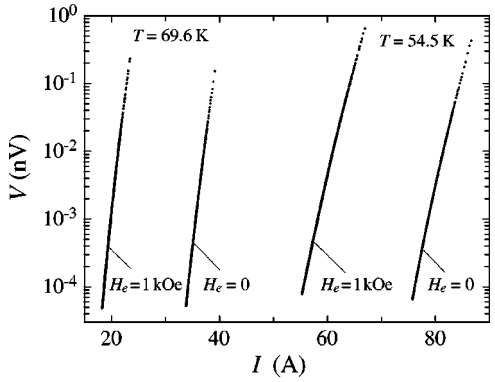

FIG. 1. Examples of *V-I* characteristics at two different temperatures.

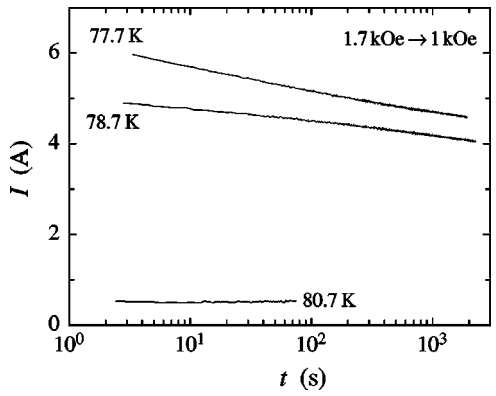

FIG. 2. Variations of the electric current I in the sample as a function of time after magnetic field step at three temperatures in the high-temperature range.

possible. The main technical obstacle is the very strong temperature dependence of the flux-creep rate at temperatures close to T_c, asking for a high stability and accuracy of the temperature control for obtaining reliable data. The desired temperature stability has been achieved by using a Platinum resistance thermometer for temperatures exceeding 30 K. With this temperature sensor the computer-based temperature controller provided a temperature stability of ± 1 mK. For lower temperatures we used a diode thermometer providing a temperature stability of ± 30 mK, sufficient in this temperature range.

Steplike changes of the external magnetic field H, oriented perpendicularly to the ring plane, were used to induce an electrical current in the ring. Three different procedures were employed, i.e., (i) switching off a field $H=1$ kOe to $H_e=0$, (ii) switching the field to a value of $H_e=1$ kOe, and (iii) switching the field to a value of $H_e=0.3$ kOe. In the last two cases both positive $(0\rightarrow H_e)$ and negative $(H_0\rightarrow H_e)$ field steps with $H_0=1.7$ kOe for the case $H_e=1$ kOe and $H_0=0.6$ kOe for $H_e=0.3$ kOe were made.

After these stepwise variations of the external field, the magnetic induction in the ring cavity B_i was monitored as a function of time t. For this purpose a LakeShore 450 Gaussmeter with a standard cryogenic Hall probe was used. From the $B_i(t)$ data, the current decay curves $I(t)$ may be calculated straightforwardly, taking into account the position of the Hall probe inside the ring cavity. Using the $I(t)$ data, the voltage around the ring sample can be calculated via $V=LdI/dt$, where $L\approx 8$ nH is the sample inductance. The primary experimental data can thus easily be converted into *V-I* characteristics of the sample. Examples of collected *V-I* curves are shown in Fig. 1.

In this kind of experiment it is very important to make sure that the current density in the sample, induced by the magnetic field step, is high enough to create the critical state throughout the sample. In this case the experimental results, represented as *V-I* curves, are practically independent of the magnitude of the field step as well as the magnetic history of the sample. We note that for $H_e=0$ and $H_e=1$ kOe, this was indeed the case for the whole covered temperature range. For $H_e=0.3$ kOe, however, the step magnitude was insufficient at low temperatures and the measurements were feasible at $T\geqslant 70$ K only.

B. Heating effects

In this kind of experiment it is also essential to avoid an overheating of the sample via Joule heating caused by the induced current. In the flux-creep regime the dissipation power is negligibly small and there is no overheating. However, during the abrupt change of the external magnetic field the induced transient current may be higher than the critical current I_c and therefore the heating effects may be considerable. During the time period of the magnetic-field step, the voltage around the sample may be estimated as

$$V=-\frac{1}{c}\frac{d\Phi}{dt}, \tag{1}$$

where c is the speed of light and Φ is the magnetic flux inside the ring cavity. In our experiments the duration of the field variation was of the order of 50 ms. This implies a voltage $V\sim 100\ \mu$V, which is more than five orders of magnitude higher than typical voltages in the flux creep regime.

Our thin-film sample has a low heat capacity and it is in good thermal contact with the substrate. Therefore the thermal equilibrium should be restored much quicker than the time given by the delay of a few seconds between the field step and the beginning of monitoring $I(t)$. In this case any overheating effects are negligible in a large part of the covered temperature range. However, at temperatures close to T_c, the situation is quite different. In this case, during the field step, the sample may be heated to above T_c and the current, induced by the field step, may decay considerably before superconductivity in the sample is restored. If the current decays too strongly, the resulting current density may not be sufficient for the creation of the critical state in the sample and the flux-creep data will be distorted.

In order to illustrate this problem we show the current decay curves for three temperatures in the high temperature range in Fig. 2. The curve corresponding to $T=77.7$ K demonstrates a slight upward curvature which is typical for flux-creep behavior. At $T=78.7$ K the situation is already different. The curvature is of opposite sign, indicating that the current density was insufficient to create the critical state. At $T=80.7$ K the current is close to zero from the very beginning and the flux-creep phenomenon is no longer reflected in

the $I(t)$ curve. In this way, overheating limits the temperature range where useful experiments of this kind may be made. Different field steps have different upper temperature limits. In our work the lowest limit is attained when the external magnetic field is switched to 1 kOe. As is illustrated in Fig. 2, in this case meaningful measurements are not possible above $T \approx 78$ K. For $H_e = 0$, the limiting temperature was about 81 K, whereas for $H_e = 0.3$ kOe, measurements up to $T \approx 83$ K were possible.

C. Magnetic induction in the sample

The important parameter in the flux-creep process is the magnetic induction B in the bulk of the sample. The magnetic-induction fixes, for instance, the vortex density. In our experiments we did not measure B and there is no way to estimate it accurately. After the magnetic field step has been applied, B must adopt a value somewhere between those that correspond to the initial and the final values of H. This is, of course, a very rough estimate, especially in the case when the external field is switched off ($H_e = 0$). A redistribution of the magnetic induction in the sample only occurs during the field step and then, in the flux-creep regime, B remains practically constant in time.

For $H_e = 0$ the magnetic induction is due to the remnant magnetization. At low temperatures, where the critical current density is practically temperature independent,[21] B should be independent of temperature as well. At higher temperatures, however, B decreases with increasing temperature, tending to zero at $T = T_c$. This uncertainty in B greatly complicates the interpretation of the experimental data at temperatures close to T_c.

If $H_e \neq 0$, the magnetic induction B is larger than the value corresponding to H_e for the negative field step and by about the same amount smaller for the positive step. In this case it is more appropriate to use the data averaged for two different field steps rather than the individual results. The averaged results thus correspond to a temperature-independent $B = 0.3$ kG or $B = 1$ kG for $H_e = 0.3$ kOe and $H_e = 1$ kOe, respectively. The averaging also considerably reduces the experimental errors, as it is discussed in more detail in Ref. 21. This is why for $H_e \neq 0$ we present only the averaged results.

III. EXPERIMENTAL RESULTS AND ANALYSIS

One of the distinct features of the magnetization relaxation in YBCO compounds is the existence of a plateau in the temperature dependence of the normalized relaxation rate $Q = d \ln M_{irr}/d \ln t$, where M_{irr} is the nonequilibrium magnetization of the sample. Such plateaus with approximately the same values of Q have been observed for different kinds of YBCO samples, including epitaxial films.[12,23,24] Figure 3 displays the temperature dependencies of $d \ln I/d \ln t$, which is an exact equivalent of Q, for our sample. We note the typical plateau in the intermediate temperature range, obviously more pronounced in the case of $H_e = 0$. It should be noted that the $\ln I$ versus $\ln t$ curves are not exactly straight lines. In this case, the value of Q depends on the time t, at which the derivative is taken. We have chosen the value of $t = 400$ s to evaluate Q for the data presented in Fig. 3.

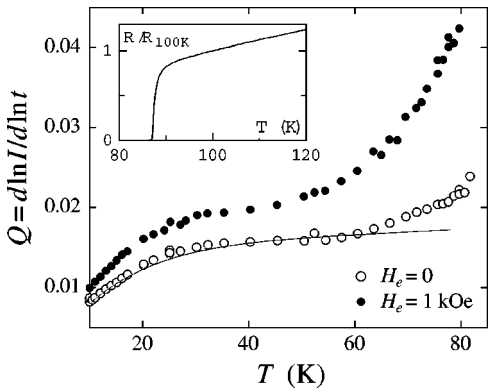

FIG. 3. The normalized relaxation rate $Q = d \ln I/d \ln t$, obtained for $H_e = 0$ and 1 kOe, as a function of temperature. The symbols represent the experimental data. The solid line represents $Q(T)$ calculated for the potential profile $u(x)$, shown in Fig. 11, for $V = 0.1$ nV. The temperature dependence of the critical current was neglected in the calculations. The calculation procedure is described in Sec. IV. The inset shows the resistive superconducting transition of the sample.

The normalized relaxation rate may also be defined as $Q = -d \ln I/d \ln V$, which is equivalent to $Q = d \ln I/d \ln t$ if both derivatives are established at the same value of current. In our case the chosen time corresponds to the voltage $V = 0.01$ nV, which is practically independent of temperature for $T \leqslant 40$ K. At higher temperatures, however, this voltage decreases with increasing temperature.

A. Scaling procedure

If the current I in the sample is less than its critical value I_c, all vortices are pinned and their motion occurs only due to either thermally activated hopping over the potential barriers or via quantum tunneling. The latter mechanism is dominant at low temperatures. For our sample the crossover from thermal activation to quantum tunneling occurs at $T \approx 10$ K. The low-temperature features have thoroughly been investigated in Ref. 21 and in the present work we consider thermal activation only. Assuming that the change of the magnetic flux in the ring cavity is due to thermally activated hopping of vortices in the sample, i.e., due to flux creep, the voltage around the sample is

$$V = V_0 \exp\left(-\frac{U}{k_B T}\right), \tag{2}$$

where

$$V_0 = \frac{\nu_0 l_{hop} B L_{creep}}{c}. \tag{3}$$

Here U is the flux-creep activation energy, k_B is the Boltzmann constant, ν_0 is an attempt frequency of the vortices to cross the potential barrier, l_{hop} is the vortex hopping distance, and L_{creep} is that length of the sample, which contributes to the flux creep.[25] L_{creep} is difficult to evaluate, however, it does not depend on current, temperature, or external

magnetic field. An electrical current creates a Lorentz force acting on the vortices F_L which tilts the potential profile, thus reducing the potential barriers for the vortex motion.

Using Eq. (2), the flux-creep activation energy may be expressed as

$$U(I) = -k_B T[\ln V(I) - \ln V_0]. \tag{4}$$

The value of the current at which $U(I)$ vanishes is a formal definition of the critical current I_c. According to Eq. (4), the parameter V_0 is equal to V at $I = I_c$.

Equation (4) offers a way to extract $U(I)$ from experiment. Unfortunately, the experimental data sets of $V(I)$ at different temperatures cover only a very narrow range of currents. An additional complication in using of Eq. (4) for evaluating $U(I)$ is that neither V_0 nor I_c are *a priori* known. In order to expand the available current range, numerous attempts to scale the data sets obtained at different temperatures have been made.[1–19] The most reliable procedure is provided by the Maley method,[1] which does not invoke any *a priori* assumptions. This method, however, is only applicable if both the flux-creep activation energy and the critical current are temperature independent. In this case, Eq. (4) implies that the *V-I* curves for different temperatures, plotted as $T \ln V$ versus I, represent different parts of the same $U(I)$ curve, but are shifted vertically with respect to each other. The application of Maley's method to experimental *V-I* curves provides a direct way to evaluate $\ln V_0$ and to determine $U(I)$. In general, however, the activation energy U and the critical current I_c are temperature dependent and the scaling of the flux-creep data turns out to be a rather complicated problem.

With this in mind we have recently developed a different approach of scaling the *V-I* curves in the flux-creep regime.[20] This procedure is based on merging the experimental *V-I* curves, using their curvature for establishing the scaling parameters. The main assumption is that the flux creep is due to thermally activated hopping of vortices or vortex bundles over potential barriers and that these hopping flux objects remain the same for all temperatures and currents. This assumption implies that an electric current does not alter the interaction of vortices with the pinning centers and therefore the potential profile for a nonzero current is obtained by a linear superposition of the zero-current potential profile and a term arising from the Lorentz force. Below we briefly discuss the essential consequences of this assumption; more details may be found in Ref. 20.

We start by considering the profile $u(x)$ of the potential energy for the vortex motion in the vicinity of one of the potential wells. The x axis coincides with the direction of the flux motion and $x = 0$ is chosen at the inflection point of the $u(x)$ function. The Lorentz force acting on vortices can be written as

$$F_L = j \frac{n \delta \Phi_0}{c}, \tag{5}$$

where j is the current density, n is the number of vortices in the moving vortex bundle, δ is the sample thickness, and Φ_0 is the magnetic-flux quantum. Taking into account the Lorentz force, we get the potential profile for a nonzero current as

$$u(x,j) = u(x,0) - xF_L. \tag{6}$$

The important implication of Eq. (6) is that for any smooth function $u(x)$ the distance between the bottom of the well and the adjacent potential maximum along the positive x axis decreases with increasing current and vanishes at $I = I_c$. This situation, early pointed out by Beasley *et al.*,[28] implies that the flux-creep activation energy is a nonlinear function of current for any reasonable shape of the potential profile.[26] This nonlinearity of $U(I)$ results in an upward curvature of the current decay curves, which may be seen in Fig. 2, and in a downward curvature of the log *V-I* curves depicted in Fig. 1.

The critical current density is reached if the potential barriers vanish. According to Eqs. (5) and (6), this results in

$$j_c = \frac{c u_c'}{n \delta \Phi_0}, \tag{7}$$

where u_c' is the maximum value of $du(j=0)/dx$. This value is reached at the inflection point, i.e., at $x = 0$. In the following we assume that not the shape, but only the amplitude of the $u(x)$ function is temperature dependent, i.e.,

$$u(x) = U_0(T) f(x) \tag{8}$$

where $U_0(T)$ is the temperature-dependent amplitude of the $u(x)$ function. Equation (8) represents the second assumption, on which our scaling procedure is based. Using both our assumption that the structure of the hopping flux object is independent of temperature and Eq. (8), the flux-creep activation energy may be written as

$$U(I,T) = U_0(T) Y(I/I_c), \tag{9}$$

where the function Y depends only on the ratio I/I_c.[20] By comparing Eq. (9) with Eqs. (7) and (8), it is obvious that both the critical current and the activation energy exhibit the same temperature dependence, given by the function $U_0(T)$.

At currents close to I_c only a small part of the $u(x)$ function in the vicinity of the inflection point is essential in the formation of potential barriers. Since $u(x)$ is virtually a linear function in this region, the validity of Eq. (8) is practically obvious. At lower currents, however, the flux-creep activation energy is determined by the features of $u(x)$ far away from the inflection point and the applicability of Eqs. (8) and (9) is difficult to justify *a priori*. As will be shown below, the analysis of our experimental results strongly indicates that the conditions expressed in Eqs. (8) and (9) are actually valid for a very wide range of currents down to $I \sim 0.1 I_c$.

In Ref. 20 it was shown that, if the flux-creep activation energy may indeed be written as a product of a temperature and a current dependent term, the following transformation occurs:

$$T_0 \ln V(I/i, T_0) = \frac{T \ln V(I,T)}{i} + A T_0, \tag{10}$$

where

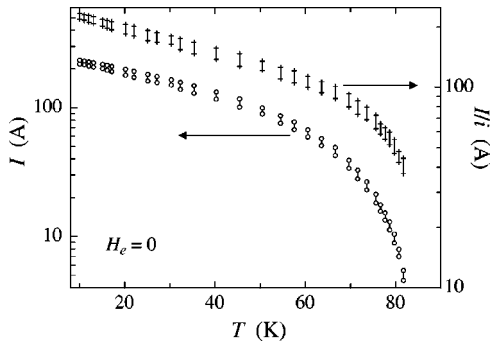

FIG. 4. Covered current ranges at many different temperatures and at $H_e = 0$. The right-hand scale is a renormalized current scale.

$$A = \left(1 - \frac{T}{iT_0}\right) \ln V_0 , \tag{11}$$

and may be used to merge the *V-I* curves at different temperatures into a single master curve. Here, $i = I_c(T)/I_c(T_0) = U_0(T)/U_0(T_0)$ and A are the scaling parameters, and T_0 is some arbitrary chosen temperature within the investigated temperature range. The resulting master curve represents the current dependence of $T \ln V$ at $T = T_0$, as if $V(I)$ could actually be measured over this extended range of currents at this single temperature. For each temperature the values of i and A can be found from the condition that the overlapping parts of the $T \ln V$ versus I curves for the adjacent temperatures match each other. It is important to recall that in this procedure we do not use the relation between i and A given by Eq. (11), but consider them as independent fitting parameters. Equation (11) is used retrospectively to check the validity of our approach.

A successful application of the proposed scaling procedure demands that the current decay measurements are made at temperatures separated by sufficiently small intervals, such as to ascertain a considerable overlap of the *V-I* curves for neighboring temperatures. Figure 4 displays the full set of the current ranges covered by the *V-I* curves at each temperature and $H_e = 0$. The left vertical scale denotes the absolute values of the current, while the right one represents the normalized values. The latter set of data demonstrates that in all cases the overlap of the *V-I* curves were sufficient to ensure a satisfying accuracy of the scaling procedure.

B. Results for $H_e = 0$ and $H_e = 1$ kOe

In this section we present the results of the scaling procedure for $H_e = 0$ and $H_e = 1$ kOe. The measurements for these two cases were made down to $T = 10$ K. The case of $H_e = 0.3$ kOe, which could only be studied at $T \geqslant 70$ K, will be discussed in the next section.

We have applied the scaling procedure according to Eq. (10) to our experimental *V-I* curves and the corresponding master curves are shown in Fig. 5. As may be seen, the outlined scaling procedure provides the corresponding master curves by a practically perfect alignment of the $T \ln V$ versus I curves obtained at different temperatures, as it is emphasized in the inset of Fig. 5.

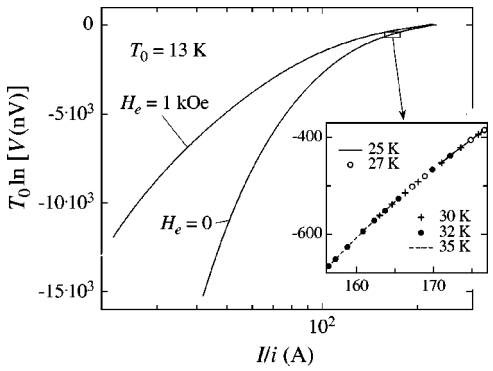

FIG. 5. Results of the scaling procedure in the form of $T_0 \ln V(T_0)$ versus I/i with $T_0 = 13$ K. The inset shows, on linear scales, the small part of the curve for $H_e = 0$ which is indicated by the rectangle in the main figure. For clarity only very few points for each temperature are displayed.

Figure 6 shows the temperature dependence of the scaling parameter i. In our approach, this plot represents the temperature dependence of the normalized critical current. Although in Fig. 5 the $T_0 \ln V$ versus I/i curves for $H_e = 0$ and $H_e = 1$ kOe are rather different, the respective $i(T)$ curves for these two cases almost coincide. The small difference between the two sets of data at higher temperatures is to be expected, when taking into account the suppression of the critical current by the external magnetic field. It is the magnetic induction B in the sample which dictates the value of the critical current. As has already been mentioned, for $H_e = 0$ we are dealing with the temperature-dependent remnant magnetization, and therefore B is not constant across the covered temperature range, but tends to zero at $T = T_c$. Somewhat simpler is the case where $H_e = 1$ kOe, corresponding to a temperature independent $B = 1$ kG. For this situation we note that $i(T)$ may very well be approximated by a simple power law

$$i(T) = 1 - (T/T_{dp})^{\mu} \tag{12}$$

across the whole covered temperature range. This is illustrated in the inset of Fig. 6, where the solid line represents the fit using the function of Eq. (12), with the fit parameters

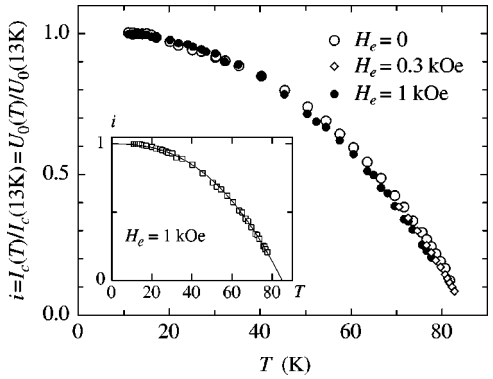

FIG. 6. The scaling parameter i as a function of temperature. The inset shows, as the solid line, a fit to the data (open squares) using Eq. (12).

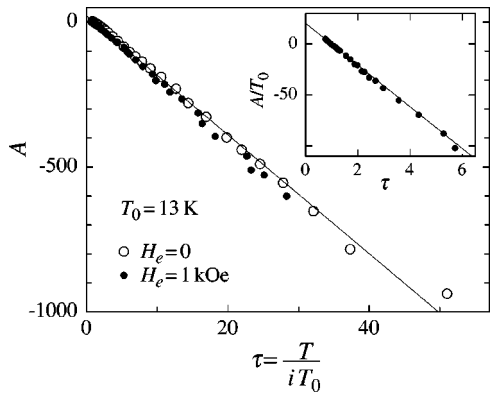

FIG. 7. The parameter A as a function of the normalized temperature $\tau = T/iT_0$ with $T_0 = 13$ K. The straight line is drawn according to Eq. (11) with $\ln[V_0(\mathrm{nV})] = 20.5$. The inset shows the low-temperature part of the plot on expanded scales.

$\mu = 2.5 \pm 0.01$ (Ref. 27) and $T_{dp} = 84.95 \pm 0.05$ K.[27] Quite surprisingly, the value of the exponent turns out to be exactly 5/2. Equation (12) implies a linear dependence of the critical current on temperature near T_{dp}.

Next we consider the temperature-dependence of the scaling parameter A. According to Eq. (11), A depends on the ratio T/i rather than the temperature alone. In Fig. 7, A is plotted as a function of $\tau = T/iT_0$. If the temperature dependence of $\ln V_0$ is negligible and our procedure is self-consistent, we expect the data to lie on a straight line. Although, according to Eq. (3), V_0 is proportional to the temperature-dependent attempt frequency, it enters Eq. (11) only as $\ln V_0$ and therefore the resulting curve is expected to deviate rather weakly from linearity. This is indeed the case, as may be seen in Fig. 7. It is also remarkable that the data for $H_e = 0$ and $H_e = 1$ kOe are rather close to each other across the entire covered temperature range. This is to be expected, however. In our model the only difference between these two cases is the different values of the magnetic induction B in the sample, which enters Eq. (11) as $\ln V_0$ [see Eq. (3)]. In this case an order of magnitude change in B will change $\ln V_0$ only by about 10%.

According to Eq. (11), the temperature dependence of $\ln V_0$ may directly be estimated from $A(t)$ as

$$\ln V_0 = -\frac{dA}{d\tau}. \tag{13}$$

Unfortunately, as one may see in Fig. 7, our accuracy is not sufficient to extract reliably the very weak temperature dependence of this parameter. At low temperatures, where the temperature dependence of $\ln V_0$ may definitely be neglected, Eq. (11) may be used to extract the value of $\ln V_0$ for the corresponding temperature range. Actually Eq. (11) provides two independent possibilities to evaluate $\ln V_0$. First, $\ln V_0 = -dA/d\tau$ [Eq. (13)] and second, $\ln V_0 = A(\tau = 0)$. Both evaluations result in the same value of $\ln V_0$, again supporting the validity of our approach.

There is yet another way to evaluate V_0. Since at low temperatures the critical current of our sample is practically temperature independent (see Fig. 6), the Maley method may be used to establish the value of $\ln V_0$ in this temperature range. This has already been done in our previous work for the temperature range between 10 and 17 K, resulting in $\ln[V_0(\mathrm{nV})] = 18.6$ for $H_e = 0$ and $\ln[V_0(\mathrm{nV})] = 20.5$ for $H_e = 1$ kOe.[21] The straight line in Fig. 7 is drawn assuming that $\ln V_0 = 20.5$, the value obtained with the Maley method for $H_e = 1$ kOe, while the data points shown in Fig. 7 were obtained by our scaling procedure, which is based on Eq. (9). As one may see in the inset of Fig. 7, the points for $H_e = 1$ kOe are very well approximated by the solid line up to $\tau \approx 5.5$, which corresponds to a temperature of about 50 K. Since the Maley method provides the value of $\ln V_0$ without any *a priori* assumptions, we consider this agreement as an important confirmation that Eq. (9), which is based on our two main assumptions, is valid.

The deviations of the high-temperature data points for $H_e = 1$ kOe from the straight line, which may be seen in Fig. 7 for $\tau \geqslant 6$, are most likely due to the temperature dependence of the attempt frequency ν_0. In the case of $H_e = 1$ kOe the increase of ν_0, according to Eq. (3), results in an increase of V_0 and $A(t)$ should deviate downward as it is indeed the case. In the case of $H_e = 0$ the situation is somewhat different. As pointed out above, in this case not only ν_0, but also the magnetic induction B is temperature dependent. Because V_0 is proportional to the product $\nu_0 B$, a more complicated behavior of the $A(\tau)$ dependence is expected in this case.

C. Results for $H_e = 0.3$ kOe

For $H_e = 0.3$ kOe the current induced by the magnetic-field step was considerably smaller than for the other two cases, thus prohibiting reliable measurements below $T = 70$ K. For the scaling procedure we have chosen $T_0 = 71$ K. As a consistency check we have also repeated the scaling procedures for $H_e = 0$ and $H_e = 1$ kOe with this value of T_0 and we compare the results obtained for all three cases.

It should be noted that in this high-temperature range the induced currents in our ring were rather small and the values of the magnetic induction, created by these currents at our Hall probe, were of the order of a few Gauss only. Such small values of the magnetic induction are difficult to measure accurately if the external magnetic field is high. That is why the measurements for $H_e = 0.3$ kOe could be made with higher accuracy than for $H_e = 1$ kOe. The data for $H_e = 0$, although accurate, are not very meaningful at high temperatures because of the uncertainty in the values of B in the case of the remnant magnetization.

Figure 8 shows $A(t)$ in the high-temperature range. One may see that a straight line is a good approximation to the data up to $T \approx 81$ K. At higher temperatures, however, there are clear upward deviations even for the case of $H_e = 0.3$ kOe, which cannot be explained by uncertainty arguments, but rather indicate the breakdown of our approach.

Figure 8 demonstrates the good agreement between the data obtained in different fields. The value of $\ln[V_0(\mathrm{nV})] = 21.8$, estimated for this temperature range slightly exceeds the value of 20.5 obtained from the analysis of the low-temperature data. We argue that it is the temperature dependence of the attempt frequency that is responsible for this

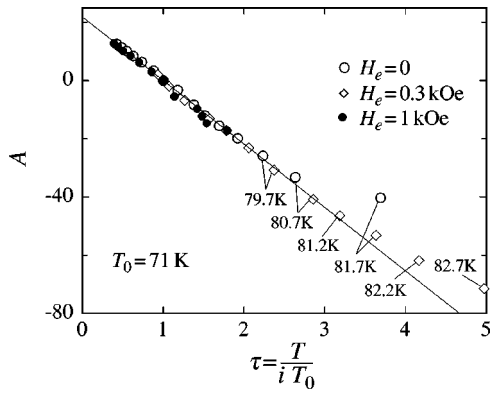

FIG. 8. The parameter A as a function of the normalized temperature $\tau=T/iT_0$ with $T_0=71$ K. The straight line is drawn according to Eq. (11) with $\ln[V_0(\mathrm{nV})]=21.8$. The temperatures related with several data points are indicated in the diagram. The data points for $H_e=0$ and $H_e=1$ kOe are shown down to $T=54$ K.

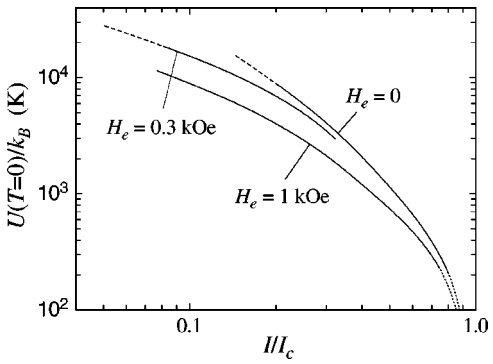

FIG. 9. $U(I/I_c)$ calculated for $T=0$. The dashed lines are calculated using data from the measurements at high temperatures, where the applicability of the scaling procedure is uncertain (see text).

difference. It should be pointed out, however, that for $H_e=0$, the deviation of the points upwards starts at lower temperatures than it is the case for $H_e=0.3$ kOe. At $H_e=0$ the magnetic induction in the sample B vanishes at $T=T_c$, which should result in a noticeable decrease of $\ln V_0$ close to T_c [see Eq. (3)]. In this case, according to Eq. (11), A at a given value of τ should increase in agreement with Fig. 8.

The scaling procedure provides, as before, the temperature dependence of the scaling parameter $i(T)$, and in this case $i=I_c(T)/I_c(71K)$. For a comparison with data in Fig. 6, the present set $i(T)$ has to be multiplied by $I_c(71K)/I_c(13K)$. Because for $H_e=0.3$ kOe the lowest achieved temperature was 70 K, $I_c(71K)/I_c(13K)$ could not be evaluated directly. However, as one may see in Fig. 6, the difference between the $i(T)$ sets for $H_e=0$ and $H_e=1$ kOe is small. Therefore there is no risk of a significant error if we equate $I_c(71K)/I_c(13K)$ for $H_e=0.3$ kOe with the arithmetic mean of the corresponding values for $H_e=0$ and $H_e=1$ kOe. The points calculated in this way are also shown in Fig. 6.

D. Evaluation of the critical current and the activation energy

As demonstrated above, the assumption that the hopping flux objects remains the same for all currents and temperatures together with Eq. (9) are sufficient for the scaling of the $\ln V$ versus I curves obtained at different temperatures. In this procedure the scaling parameter i represents the temperature dependence of the normalized critical current, but the absolute value of I_c remains unknown. Below we show that the same assumptions are also sufficient to establish the absolute value of the critical current from the experimental data. The approach that we consider in this section was first used by Beasley *et al.*[28] At currents close to I_c only a small part of the $u(x)$ function in the vicinity of $x=0$ represents the essential part of the potential barrier. In this case $u(x)$ may be expanded in a Taylor series about the point $x=0$. Taking into account that $d^2u/dx^2=0$ at $x=0$ and keeping only the first two nonzero terms,

$$u(x)=u_c'x-bx^3. \tag{14}$$

Using this analytical expression for $u(x)$, one obtains

$$U(I/I_c)=\frac{4(u_c')^{3/2}}{3\sqrt{3b}}(1-I/I_c)^{3/2}. \tag{15}$$

Hence the current dependence of the activation energy for $(1-I/I_c)\ll 1$ should follow Eq. (15), independently of the particular shape of $u(x)$. In this case, one can use Eq. (15) together with Eq. (4) to estimate I_c, $\ln V_0$, and b from the V-I data. In our already cited previous publication the high current part of the $\ln V$ versus I curve was fitted in this way.[20] This procedure worked reasonably well, but introducing three fitting parameters led to a substantial uncertainty. Now we have rather accurate estimates of $\ln V_0$, as obtained using Maley's method in Ref. 21, and therefore we can use the same fitting procedure as in Ref. 20 but with only two fitting parameters. In this way we obtain $I_c(H_e=0)=290$ A and $I_c(1\ \mathrm{kOe})=301.5$ A, very similar values, as expected. These are the values for $T=T_0=13$ K. Since I_c is practically temperature independent at low temperatures, these values may safely be considered as the critical currents for $T=0$.

Since $I_c(T=0)$ and $\ln V_0$ are now known, we may apply Eq. (4) to calculate $U(I/I_c)$ from the master curves presented in Fig. 5.[29] The results are shown in Fig. 9 on double logarithmic scales. As mentioned above, the data at the highest temperatures cannot be described by our approach. Therefore the corresponding parts of the $U(I/I_c)$ curves, still calculated in the same way, are indicated by the dashed lines. The different parts of the $U(I/I_c)$ curves presented in Fig. 9 are calculated from the V-I characteristics measured at different temperatures. As we saw, the parameter $\ln V_0$ is slightly temperature dependent, however, the exact value of $\ln V_0$ is only important for currents close to I_c and hence low activation energies, i.e., for the analysis of measurements made at low temperatures. This justifies the use of the low-temperature value of $\ln V_0$ for the whole temperature range.

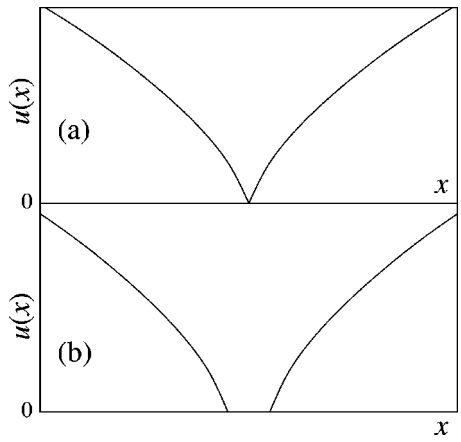

FIG. 10. Schematic plots of $u(x)$ near the bottom of the potential well which have been used in our calculations (see text).

E. Reconstruction of the shape of the potential barriers

In our approximation, there is a direct connection between the profile of the potential barriers $u(x)$ in real space and $U(I/I_c)$. The function $u(x)$ may be derived from the $U(I/I_c)$ data as they follow from experiment. However, $u(x)$ can be found unambiguously only if some additional assumptions about its features are made. Here, as well as in our previous work,[20] we assume that the shape of the $u(x)$ function is as illustrated in Fig. 10(a), i.e., the point where du/dx has its maximum corresponds to the bottom of the potential well. The somewhat more realistic potential shown in Fig. 10(b) does not alter the result of the calculation procedure.

The calculation procedure is described in detail in Ref. 20. The value of $u_c'/n \approx 2000$ K/Å can be estimated from the critical current density using Eq. (7). The results of the calculations are presented in Fig. 11 as a function of the product nx, with n being the number of the vortex lines in the hopping vortex bundle. We have postulated that n does not depend on current and temperature and the experimental results, presented in this work, strongly indicate that this is indeed the case. There is no way to deduce n directly from the experimental data. Since, however, our analysis, based on the fact that the hopping flux object remains the same, is rather successful for this wide range of temperatures, it seems most likely that we are dealing with a hopping of single vortices, i.e., $n=1$. The $u(x)$ functions shown in Fig. 11 represent pinning potentials for three different values of the applied magnetic field. These pinning potentials include not only the interaction of the vortex line with one particular pinning center, but also with other vortices. Note that only the solid lines in Fig. 11 represent reliable results. The dashed lines are obtained by formally using our approach in the temperature range where its application is not really valid.

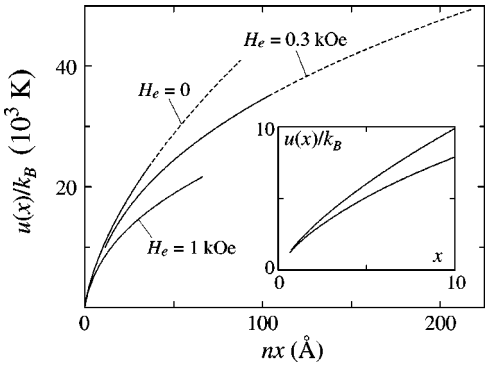

FIG. 11. The potential profiles for zero current, calculated from $U(I/I_c)$. The dashed lines correspond to the dashed lines in Fig. 9. The inset emphasizes the behavior of $u(x)$ for small x. The solid lines are calculated from the experimental data. The dotted line is an extrapolation of $u(x)$ using Eq. (14).

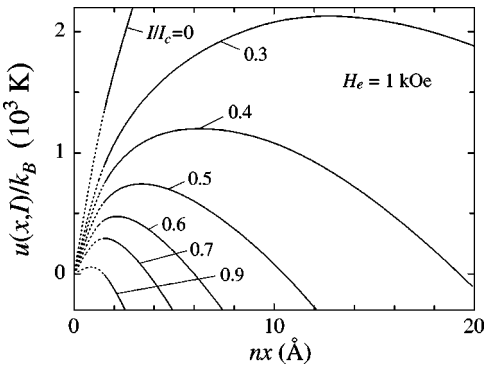

FIG. 12. Calculated variations of the potential profile, shown in Fig. 11 for $H_e=1$ kOe, with increasing current. The corresponding values of I/I_c are indicated near the curves. The dotted lines indicate extrapolations using Eq. (14).

The electric current does not change the vortex interaction with the pinning centers or other vortices, but it causes a Lorentz force to act on the vortices. This force tilts the potential profile as is illustrated in Fig. 12. This figure clearly demonstrates that the position of the maximum of the potential barrier moves closer to the bottom of the potential well with increasing I/I_c. Figure 13 shows the x position of the maxima of $u(x,I)$ as a function of I/I_c. It may be seen that for most of the investigated current range, the extension of the potential barriers is limited to small values of x.

IV. DISCUSSION

In this work we have applied a different scaling procedure, described in Ref. 20, to analyze the experimental flux-

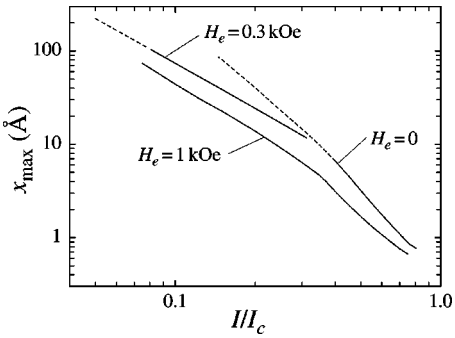

FIG. 13. The position of the potential barrier maxima as a function of I/I_c. The solid, dashed, and dotted lines are calculated from the corresponding curves shown in Fig. 11. Here we assume that the number n of vortices in the moving flux bundle is 1 (see text).

creep data obtained for a superconducting YBCO film in a wide range of temperatures. The two basic assumptions on which the scaling procedure relies are (i), the hopping flux object remains the same for all currents and temperatures and (ii), the temperature dependence of the flux-creep activation energy can be described by Eq. (9), implying that not the shape, but only the amplitude of potential barriers is temperature dependent.

With these assumptions, our approach does not allow any freedom in the treatment of the experimental data. The two scaling parameters i and A of Eq. (10) and their variations with temperature are unambiguously determined by the shape of the experimental V-I curves. It is to be noted that Eq. (11) provides the possibility to verify the consistency of the approach. Although the parameters i and A are solely evaluated by using Eq. (10), they should also obey Eq. (11), if our approach makes sense. As one may see in Figs. 7 and 8, the relation between i and A indeed follows Eq. (11) from the lowest investigated temperature of 10 K up to $T \approx 81$ K. Taking into account that in this temperature range $\tau = T/iT_0$ changes by almost a factor of 60, we consider the validity of Eq. (11) in this wide range of τ as unequivocal evidence that the chosen approach is meaningful and that Eq. (9) is indeed valid in the corresponding range of currents. A similar approach has successfully been applied in the analysis of the same type of V-I data at low temperatures, where quantum tunneling of vortices is predominant.[21]

Small deviations of the experimental points from the straight line given by Eq. (11), which may be seen in Fig. 8 for the highest investigated temperatures and $H_e = 0.3$ kOe, indicate that our approach is not adequate for describing the flux-creep process close to T_c. Taking into account the simplicity of the assumptions that have been made, this failure is not surprising at all. We believe that the most likely reason for these deviations is that Eq. (9) does not correctly describe the temperature dependence of the activation energy for temperatures in the vicinity of T_c. As has already been discussed, the experimentally available range of the I/I_c values decreases with increasing temperature. It means that at high temperatures we get the low current part of $U(I/I_c)$, which is mainly determined by the behavior of the $u(x)$ function far away from the bottom of the potential well. In other words, at high temperatures the flux-creep activation energy is determined by $u(x)$ at large x, while at low temperatures $u(x)$ at small values of x is essential. It is not obvious that our assumption expressed in Eq. (8) is valid for large x. As we have seen, our description of the flux-creep process breaks down for $T > 81$ K (Fig. 8). At $T = 81$ K, the top of the potential barrier is located at a distance x_{max} approximately 100 Å away from the bottom of the potential well (Fig. 13). Comparing this distance with the coherence length $\xi(T = 81\ \mathrm{K}) \approx 50$ Å,[30] we may therefore conclude that Eq. (8) provides an adequate description of the $u(x)$ function up to $x \approx 2\xi(T)$.

As has been shown in the inset of Fig. 6, $I_c(T)$ can very well be approximated by Eq. (12). This is a rather unexpected result. One may argue that close to T_c, where the Ginzburg-Landau (GL) theory is applicable, $I_c(T)$ should be proportional to $H_{cm}\xi(T) \sim (1 - T/T_c)^{3/2}$, where H_{cm} is the thermodynamic critical field.[31,32] This means that I_c should vanish at T_c, which is about 2 K higher than T_{dp}. In addition the GL theory provides a different temperature dependence of I_c in this regime than is dictated by Eq. (12). However, this disagreement may just as well be fictitious because for $H_e = 1$ kOe we have established the $I_c(T)$ curve up to $T \approx 78$ K only, and we cannot exclude that there will be a change of the T dependence of I_c at higher temperatures. Although we do not have any experimental indication for such a change, it is important to state that our results do not exclude this possibility.

We now return to the temperature dependence of the normalized relaxation rate Q, which is shown in Fig. 3. In our approach all the features of the flux-creep process follow from the profiles of the potential barriers, which are shown in Fig. 11. Using these profiles, one may also calculate $Q(T)$. In an exact calculation, the temperature dependence of the critical current should be taken into account. But even our simplified calculation, neglecting the temperature dependence of I_c gives a fairly good account of $Q(T)$, as may be seen from the solid line shown in Fig. 3. It thus turns out that the appearance of a plateau in $Q(T)$ may be traced back to a very simple shape of the potential barrier and no additional assumptions are needed to explain this, at first glance, very astonishing $Q(T)$ curve. This kind of $Q(T)$ curves is a common feature of different YBCO material, including not only films, but also flux-grown and melt-processed crystals.[12,23,24] The close similarity of the $Q(T)$ curves for all these materials leads to the natural conclusion that the plateau in the $Q(T)$ curves must have a common origin, implying that the profiles of the potential barriers in different YBCO materials are similar. There are also sufficient physical grounds for such a conclusion. The potential profile for a chosen pinning center is determined by the structure of the vortex line. The distribution of the order parameter near the vortex core and the distribution of the magnetic field around the vortex line are the most important ingredients. Because the coherence length ξ and the magnetic-field penetration depth λ are the relevant material parameters, it seems quite likely that the profiles of the potential barriers are similar in different samples of the same compound. We conclude that the particular combination of ξ and λ in YBCO compounds is the reason for the formation of a plateau in $Q(T)$.

In this paper we have used $U(I/I_c)$ to calculate the profile of potential barriers as illustrated in Figs. 11 and 12. On the other hand, it is well known that HTSC samples are not uniform and one should expect that different barriers have different shapes. In this situation, the physical relevance of the potential profiles calculated in the way outlined above is not obvious. In order to clarify the situation, we consider the flux-creep process in more detail. There are very many different trajectories by which the vortices are allowed to cross the ring sample. It is obvious, however, that only those trajectories containing the lowest potential barriers will actually be used. There are also many different potential barriers along each trajectory, but the very few with the largest amplitudes are essential in limiting the vortex motion. In our experiments an average value of U/k_BT is 25. This ratio, according to Eq. (2), is related with the probability of the

thermally activated hopping. For such large values of U/k_BT, even very small variations of the amplitude of U between different barriers result in a considerable difference in the probability of hopping.

In the ring geometry, the evaluation of the number N of vortices which are leaving or entering the ring cavity per second is straightforward. Using Eq. (1) and taking into account that the experimentally accessible voltages range between 10^{-4} and 1 nV, we get N between 50 and 5×10^5 s^{-1} for the lowest and the highest voltage, respectively. The value of N for low voltages is only 50 vortex lines per second and it is difficult to imagine that many different trajectories are used in this case. Most likely all these vortices cross the sample along the easiest way and on this trajectory, only the barrier with the largest amplitude determines the actual flux-creep rate. In our approach we assume that the $u(x)$ function which describes the potential profile remains the same, independently of the vortex transfer rate. This is why it is important to verify whether one single trajectory is also sufficient for transferring a much larger number of vortices, corresponding to $V=1$ nV. For $B=1$ kG the distance between vortices is of the order of 10^{-5} cm. This implies an average vortex velocity $w\sim5$ cm/s, if we force all 5×10^5 vortices to follow the same trajectory across the sample in one second. This value of w is rather low and there is no reason to expect that a single trajectory would no longer suffice for the transfer of vortices with increasing V in this voltage range.

An important consequence of this line of thoughts is that the analysis of flux-creep rates provides information only about one particular pinning center, which represents the highest potential barrier for the vortex motion on the energetically most favorable trajectory across the sample. This is true not only for our experiments, but for all measurements of magnetization relaxation. It should be noted that at voltages a few orders of magnitude higher but still corresponding to the flux-creep regime, nonlinear effects connected with the vortex motion may already be important. In this case one trajectory will not be sufficient for transferring all the vortices across the sample and, still in the flux-creep regime, a crossover from one to several trajectories with increasing voltage is expected. Such a transition is expected to be indicated by a corresponding alteration of the shape of the V-I curves.

V. SUMMARY AND CONCLUSIONS

We present a detailed experimental study of flux-creep rates in a ring-shaped superconducting YBCO film. A very wide range of temperatures between 10 and 83 K has been investigated. It is shown that all the details of the flux-creep process can be traced back to simple thermally activated hopping of vortices or vortex bundles over potential barriers with the hopping flux object remaining the same for all currents and temperatures. This is, in fact, the simplest possible approach for describing the flux-creep phenomenon. Using a recently developed scaling procedure,[20] we have succeeded in extracting the current dependence of the flux-creep activation energy (Fig. 9) and the temperature dependence of the critical current (Fig. 6) from the primary V-I data. In the whole covered temperature range, the temperature dependence of the critical current $I_c(T)$ can very well be approximated by a simple power law [Eq. (11)]. The current dependence of the activation energy $U(I/I_c)$ is then used to reconstruct the profiles of the potential barriers in real space (Figs. 11 and 12). It is important to emphasize that the outlined scaling procedure passes internal consistency checks and it appears that the proposed approach adequately describes the real flux-creep process.

In practically all previous reports where scaling procedures have been used to extract $U(I)$ from flux-creep data, the condition imposed by Eq. (9) has been adopted. Therefore the main difference between our approach and other models is that, instead of complicated assumptions, we consider the simplest possible case of the vortex hopping. It is also important that we have chosen the shape of the experimental $\ln V$ versus I curves as a criterion for deriving the scaling parameters. This renders our approach free from any additional assumptions.

[1] M. P. Maley, J. O. Willis, H. Lessure, and M. E. McHenry, Phys. Rev. B **42**, 2639 (1990).

[2] B. M. Lairson, J. Z. Sun, T. H. Geballe, M. R. Beasley, and J. C. Baravman, Phys. Rev. B **43**, 10 405 (1991).

[3] M. E. McHenry, S. Simizu, H. Lessure, M. P. Maley, J. Y. Coulter, I. Tanaka, and H. Kojima, Phys. Rev. B **44**, 7614 (1991).

[4] D. Shi and S. Salem-Sugui, Jr., Phys. Rev. B **44**, 7647 (1991).

[5] P. J. Kung, M. P. Maley, M. E. McHenry, J. O. Willis, and J. Y. Coulter, Phys. Rev. B **46**, 6427 (1992).

[6] S. Sengupta, D. Shi, Z. Wang, M. E. Smith, and P. J. McGinn, Phys. Rev. B **47**, 5165 (1993).

[7] S. Sengupta, D. Shi, Z. Wang, M. E. Smith, S. Salem-Sugui, Jr., and P. J. McGinn, Phys. Rev. B **47**, 5414 (1993).

[8] J. R. Thompson, Y. R. Sun, L. Civale, A. P. Malozemoff, M. W. McElfresh, A. D. Marwick, and F. Holtzberg, Phys. Rev. B **47**, 14 440 (1993).

[9] H. G. Schnack, R. Griessen, J. G. Lensink, and H. H. Wen, Phys. Rev. B **48**, 13 178 (1193).

[10] H. Theuss and H. Kronmller, Physica C **229**, 17 (1994).

[11] S. H. Chun, S. H. Moon, Y. Chong, and Z. G. Khim, Physica C **235-240**, 2919 (1994).

[12] H. H. Wen, Z. X. Zhao, R. J. Wijngaarden, J. Rector, B. Dam, and R. Griessen, Phys. Rev. B **52**, 4583 (1995).

[13] H. H. Wen, H. G. Schnack, R. Griessen, B. Dam, and J. Rector, Physica C **241**, 353 (1995).

[14] J. J. Sun, B. R. Zhao, L. Li, B. Xu, J. W. Li, S. Q. Guo, and B. Yin, Physica C **291**, 257 (1997).

[15] Y. Yu, X. N. Xu, Z. Y. Zheng, X. Jin, and X. X. Yao, Supercond. Sci. Technol. **10**, 568 (1997).

[16] H. H. Wen, P. Ziemann, H. A. Radovan, and T. Herzog, Physica C **305**, 185 (1998).

[17] J. Jung, H. Darhmaoui, and H. Yan, Supercond. Sci. Technol. **11**, 973 (1998).
[18] E. Moratakis, M. Pissas, G. Kallias, and D. Niarchos, Supercond. Sci. Technol. **12**, 682 (1999).
[19] H. H. Wen, Z. X. Zhao, S. L. Yan, L. Fang, and M. He, Physica C **312**, 274 (1999).
[20] I. L. Landau and H. R. Ott, Physica C **331**, 1 (2000).
[21] I. L. Landau and H. R. Ott, Physica C **340**, 251 (2000).
[22] I. L. Landau and H. R. Ott, Phys. Rev. B **61**, 727 (2000).
[23] Y. Yeshurun, A. P. Malozemoff, and A. Shaulov, Rev. Mod. Phys. **68**, 911 (1994).
[24] A. P. Malozemoff and M. P. A. Fisher, Phys. Rev. B **42**, 6784 (1990).
[25] In the flux-creep regime the resistance of the sample depends exponentially on j/j_c and even small fluctuations of the sample cross section or the critical current density reduce L_{creep} significantly to below the total length of the sample.
[26] The activation energy is a linear function of current only for triangular or trapezoidal potential barriers.
[27] These error margins are errors of approximation only and do not include experimental errors and additional errors introduced by the scaling procedure.
[28] M. R. Beasley, R. Labusch, and W. W. Webb, Phys. Rev. **181**, 682 (1969).
[29] For the case of $H_e=0.3$ kOe, $I_c(T=0)$ was estimated as an arithmetic mean of the corresponding values for $H_e=0$ and $H_e=1$ kOe.
[30] G. Blatter, M. V. Feigelman, V. B. Geshkenbein, A. I. Larkin, and V. M. Vinokur, Rev. Mod. Phys. **86**, 1125 (1994).
[31] Y. Yeshurun and A. P. Malozemoff, Phys. Rev. Lett. **60**, 2202 (1988).
[32] M. Tinkham, Phys. Rev. Lett. **61**, 1658 (1988).